MATERIALE PLASTICE
https://revmaterialeplastice.ro
https://doi.org/10.37358/Mat.Plast.1964

Infill Density Effect on the Flexural Behavior of FFF-Based AM Polylactic Acid Parts

ION MIRON[1], CRISTINA VĂLEAN[2], EMANOIL LINUL[1]*

[1] Department of Mechanics and Strength of Materials, Politehnica University Timisoara, Mihai Viteazu Bv., No. 1, Timisoara, 300222, Romania

[2] Research Institute for Renewable Energies (ICER), Politehnica University Timisoara, Musicescu Gavril Str., No. 138, Timisoara, 300774, Romania

Abstract: *Fused Filament Fabrication (FFF) is an additive manufacturing process with wide use. However, the optimization of certain parameters presents some uncertainties in the FFF process. In the present study, the effect of infill density (ID) on the flexural behavior of Polylactic Acid (PLA) parts printed by the FFF process was investigated. The experimental tests were performed on rectangular parts, according to the ISO 178 standard, with a test speed of 5 mm/min. Parts with several IDs in the 20–100% range were 3D printed, analyzed, and tested. Every sample was subjected to dimensional and mass analyses before the experimental tests. After testing, the failure mechanisms were highlighted depending on the ID. It was found that the ID of the printed parts strongly influences the flexural characteristics (elastic, strength, strain, and energy absorption). However, using the specific properties (specific modulus and specific strength), it was noted that 20%-ID is the optimal density for such AM structures. Slight dependencies on IDs were recorded for dimensional accuracy. It was obtained that at low IDs (<40%), the FFF-printed parts show a quasi-brittle fracture, and with its increase (IDs > 60%), a slight plastic deformation was observed.*

Keywords: *Fused filament fabrication, polylactic acid, flexural behavior, infill density*

1. Introduction

Additive Manufacturing (3D printing) has become increasingly popular over the past decades [1–3]. The increase is given by the multiple advantages that this technology offers [4,5]. Using computer-aided design (CAD) software, this process involves creating a 3D model, which is then built by successively adding material layer by layer using a series of cross-sectional slices [6–8]. The Fused Filament Fabrication (FFF) is a technique of 3D printing that is widely used in research due to its cost-effectiveness, versatility, and non-laser application [9,10].

Most of the data are related to traction, but there are also studies with reference to compression or bending behavior [11,12]. Krzikalla et al. [13], using a three-point bending test, investigated the flexural properties (experimental and numerical) of FFF long carbon fiber-reinforced composites with a polymeric matrix of Onyx. The study found that the reinforced layers distribution is essential over the fiber content. Maqsood and Rimašauskas [14] combined continuous carbon fiber with short carbon thermoplastic material and studied the phenomenon of delamination instead of breakage during the bending test. The cause was an insufficient and poor interfacial linkage between the reinforcement and matrix material, but optimized printing parameters could enhance the effectiveness of the process.

Analysis of parameters characteristic of 3D printing, such as type of infill, infill density, and interaction of the factors was performed by González Rebenaque et al. [15]. One of the conclusions was that a better resistance to bending is obtained at higher infill density, but it also leads to an increase of the printing time. In a study conducted by Yousefi Kanani and Kennedy [16], a variety of distinct sandwich configurations made using foamable polymer filaments were tested, and the obtained results

email: emanoil.linul@upt.ro

were compared to foamed and non-foamed beams. The research concluded that yield load, stiffness, and maximum load of composite beams with foamed cores and non-foamed face sheets exhibit significantly higher values compared to non-foamed PLA-printed beams. Atakok et al. [17] investigate FFF printed PLA and recycled PLA specimens with different parameters, such as layer thicknesses and occupancy rates, using the Taguchi methodology. Izod impact, tensile and flexural tests were performed. Layer thickness was shown to be the most influential parameter for mechanical properties, and the optimal configuration appeared to be, for all test results, 70%, 0.25 mm and PLA. There are many materials used for FFF printing and each has different mechanical properties, respectively, suitable for different applications, reported by Djokikj et al. [18].

As can be seen in the literature, a variety of process parameters influence the performance of the material extruded parts. This is why, in our investigation, we kept all the process parameters the same to compare exactly the effect of infill density on flexural performance. In order to find optimal density, we used not only classical characteristics (strength, energy absorption, and strain) but also the specific ones too (specific flexural modulus and specific strength).

2. Materials and methods

2.1. Materials and specimens

In the present investigation, Polylactic Acid (PLA) was used, which is bio-based thermoplastic popular for its printability, superior mechanical strength, low melting temperature, and low costs [19–21]. This material is used in many industries, such as packaging, agriculture, textiles, electronics, transportation, and the biomedical industry (Figure 1) [22–24].

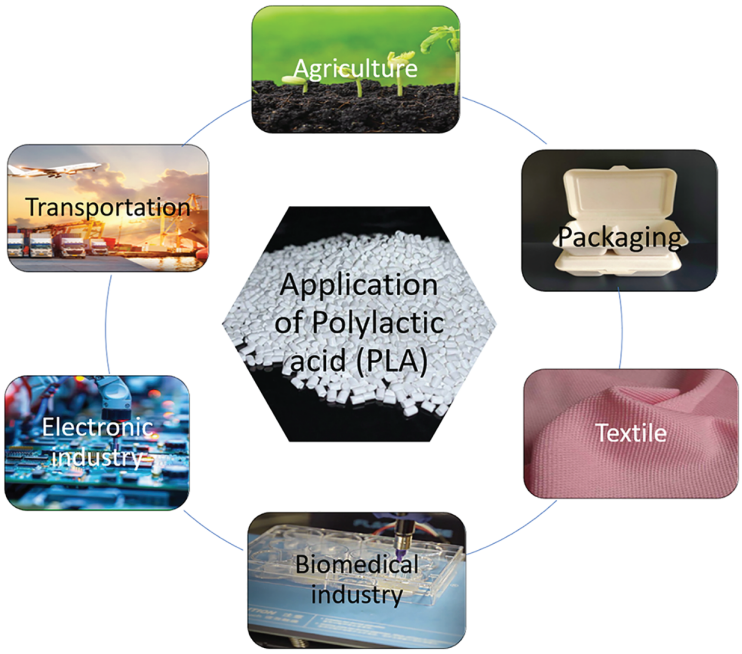

Figure 1. Industries that use polylactic acid

For obtaining the 3D printed samples through FFF technology, the orange PLA filament was used (with an initial diameter of 1.75 mm).

A 3D CAD model of the sample was designed in CATIA V5®® (v2016, Dassault Systèmes) software. The geometry was taken from ISO 178 standard [25]: width of 10 ± 0.2 mm, length of 80 ± 2 mm, and height of 4 ± 0.2 mm (Figure 2c).

The CAD part was saved as *.stp* file and introduced in the printer software. The printer used for preparation of the samples was Prusa i3 MK3 (Figure 2a). A total of 4 samples of each infill density were printed (Figure 2b). Table 1 lists the main printing parameters.

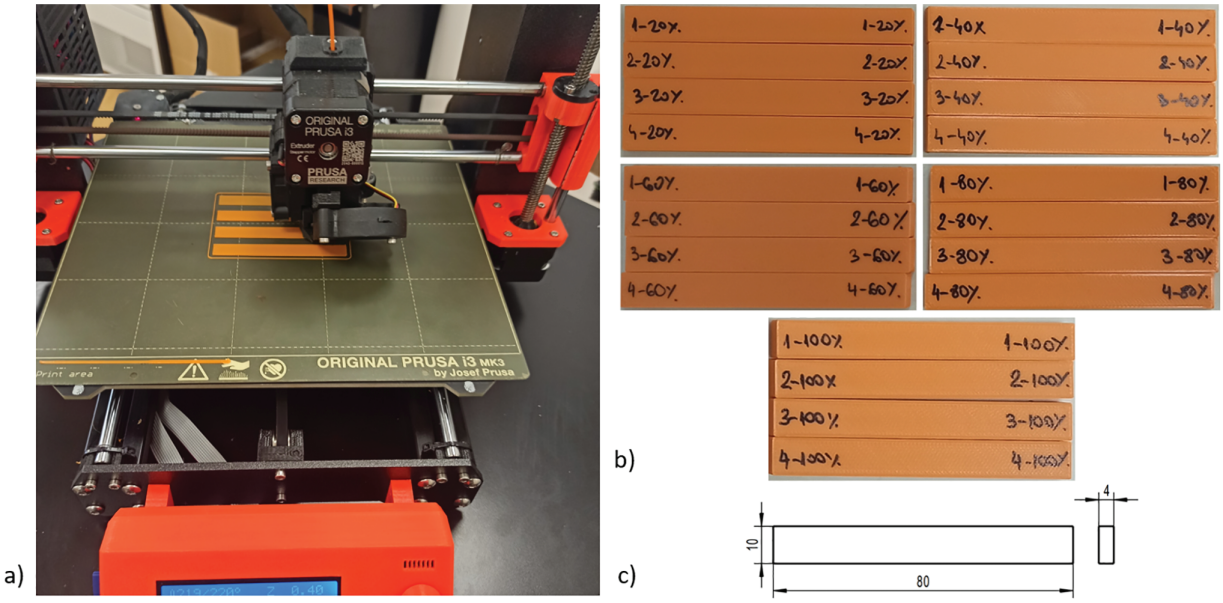

Figure 2. Prusa i3 MK3 printer (a), manufactured parts (b), and flexural part geometry, in mm (c)

Table 1. Printing parameters

Parameter	Unit	Value
Layer thickness	[mm]	0.20
Top solid layers	[-]	2
Bed temperature	[°C]	42
Number of outer layers	[-]	2
Nozzle diameter	[mm]	0.6
Nozzle temperature	[°C]	220
Bottom solid layers	[-]	2
Print speed	[mm/s]	20
Extruder quantity	[-]	single
Printing orientation	[°]	0
Travel speed	[mm/s]	100
Infill pattern	[-]	Rectilinear
Infill density	[%]	20, 40, 60, 80, 100

2.2. Methods

To assess the flexural performance of the developed composite specimens, a three-point bending test was conducted in accordance with the ISO 178:2019 standard [25] for determining flexural properties of rigid and semi-rigid plastics. All tests were carried out under controlled laboratory conditions, at a temperature of (23 ± 2)°C and relative humidity of (50 ± 5)%, in compliance with standard testing environments specified for polymer-based materials. The specimens were positioned on two parallel

supports with a span-to-depth ratio of 16:1, as required by the standard, to ensure pure bending in the central region and minimize shear influence. The experimental setup, including fixture geometry, loading configuration, and specimen alignment, is shown in Figure 3.

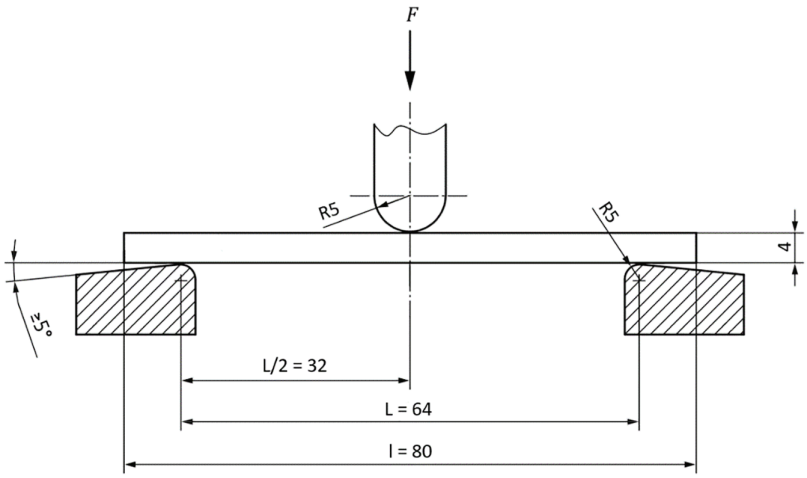

Figure 3. Experimental setup according to ISO 178 standard [25], in mm

The flexural tests were performed using a constant test speed of 5 mm/min, on 5 kN Zwick Roell testing machine. Figure 4 shows the experimental setup with the sample positioned in the machine, before the test (Figure 4a) and after the test (Figure 4b). Special attention was given to avoid specimen slippage or misalignment, which can significantly affect the accuracy and repeatability of results.

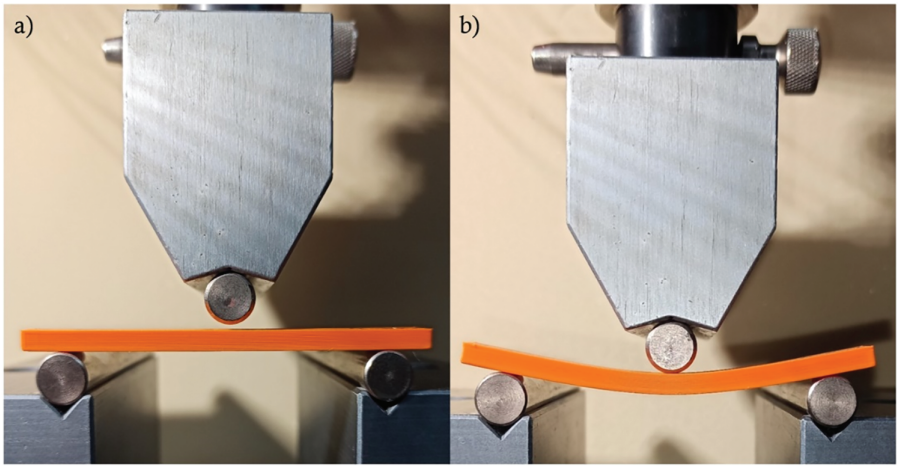

Figure 4. FFF-printed sample before (a) and during (b) the 3-point bending test

Using Eq. (1), the flexural strength was determined [22].

$$\sigma_f = \frac{3PL}{2bh^2} \tag{1}$$

where σ_f is flexural strength, L is support span (in mm), P is load at a given point on the force-displacement curve (in N), b is width of tested specimen (in mm), and h is thickness of tested specimen (in mm).

3. Results and discussions

After the manufacturing process, all the samples were measured and weighed. Dimension relative error is presented in Figure 5a. As we can see, the biggest error (0.9%) was obtained for the width values. The width error is decreasing from lower ID to the highest one, but the thickness error is the same for both infill densities and doesn't seem to follow any trend. Length error is the smallest one and is distributed randomly. Deviations recommended by the ISO 178:2019 standard [25] shall not be more than 2% of the thickness and 3% of the width of the specimen.

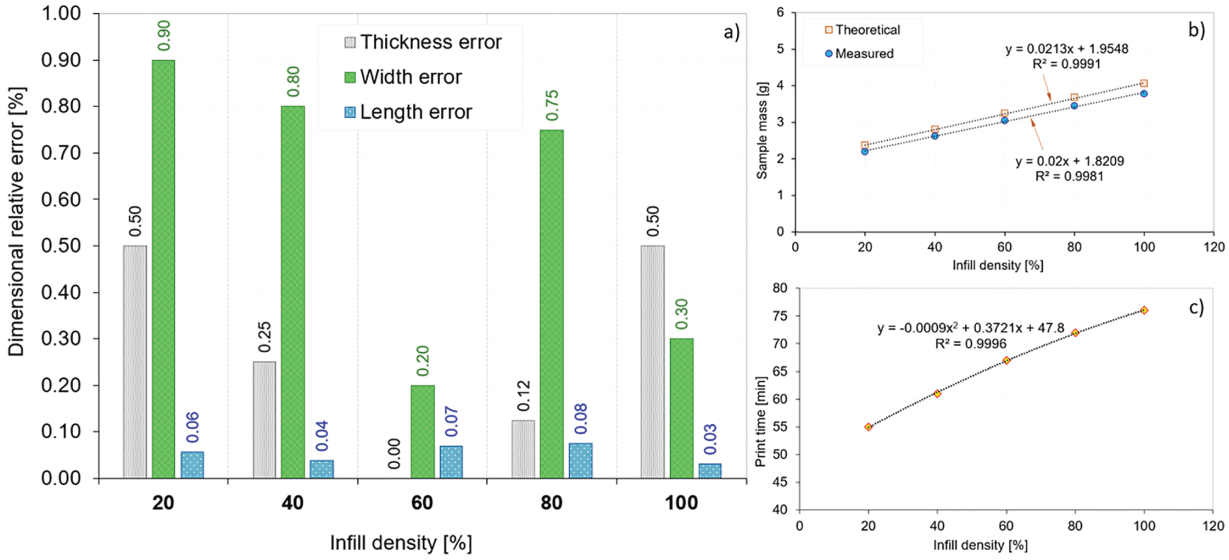

Figure 5. Dimension relative error (a), theoretical and measured mass (b), and print time (c)

The mass of the samples was estimated by the software and measured after the printing, resulting in a real mass that is lower than the theoretical one by 6.5% (Figure 5b). Both are increasing linearly with the increase in ID, according to the Eqs. (2) and (3) for theoretical and measured mass, respectively.

Printing time was recorded from the printer software. Figure 5c is illustrated that print time is growing polynomial with a minimum of 55 min for 20%-ID and maximum of 76 min for 100%-ID.

$$y = 0.0213 \cdot ID + 1.9548, \; with \, R^2 = 0.9991 \tag{2}$$

$$y = 0.02 \cdot ID + 1.8209, \; with \, R^2 = 0.9981 \tag{3}$$

In Figure 6a, it is shown that all types of ID have a clear linear-elastic zone. The 20%-ID has a quasi-brittle fracture right at the point of maximum stress. Looking at the 40%-ID curve, we can see how material starts to flow. The 60%-ID curve has an even bigger plastic zone, but still the fracture occurs at the point of maximum strength. The trend of increased plastic zone continues up to 100%-ID sample, which has a clearly ductile fracture with a big plateau of plastic deformation. As we can see in Figure 6b, the energy absorption (EA) showed increases from 1.309 MJ/m^3 for 20%-ID to 5.265 MJ/m^3, which is the biggest increase among the investigated properties (75.1%).

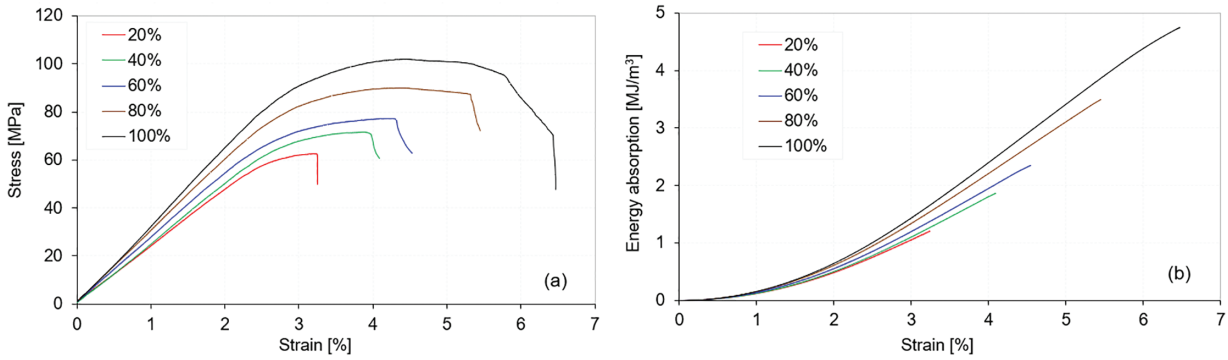

Figure 6. Stress-strain (a) and energy absorption-strain (b) curves of FFF-printed samples

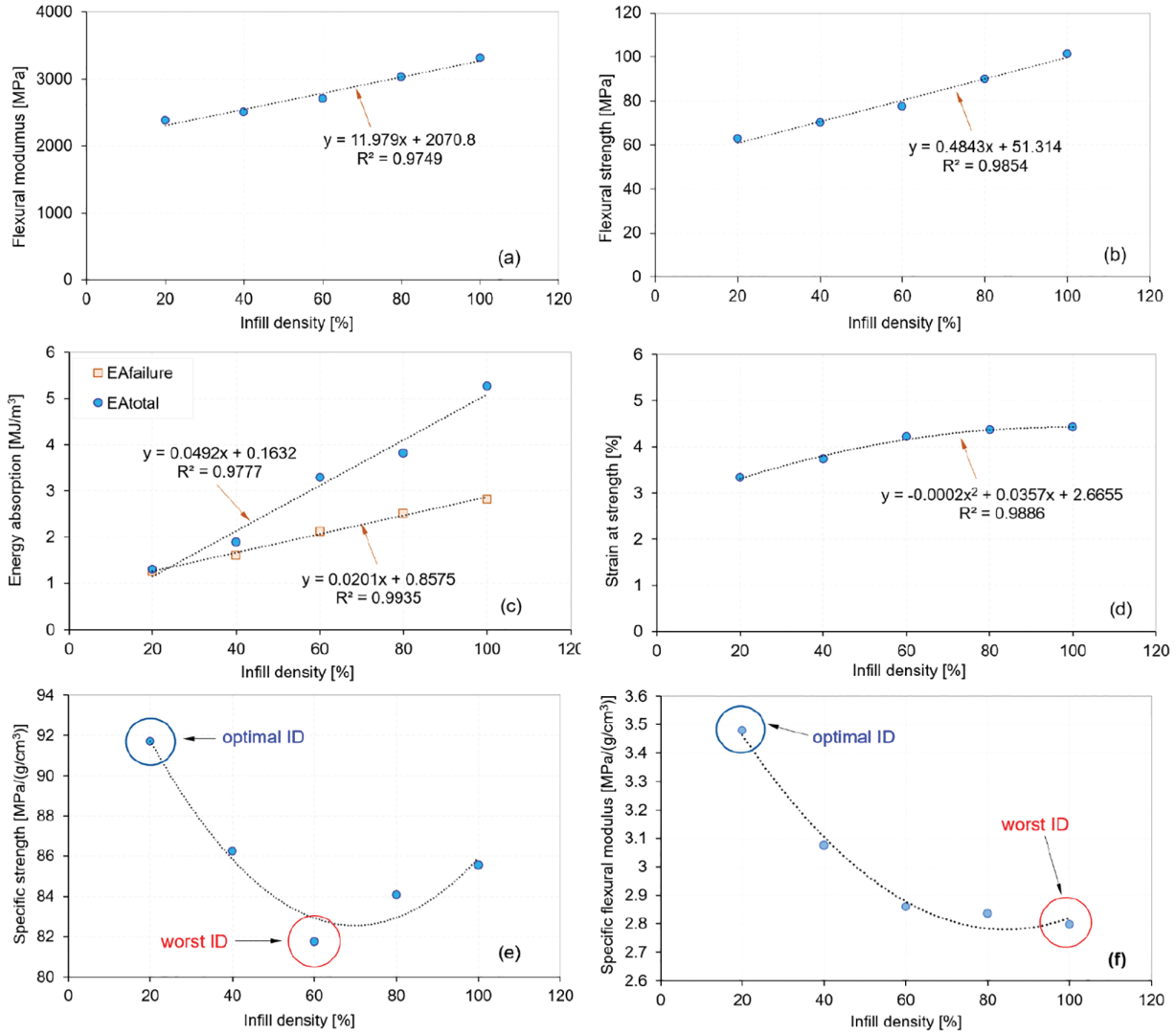

Figure 7. Mechanical characteristics of FFF-printed samples: flexural modulus (a), flexural strength (b), energy absorption (c), strain at strength (d), specific strength (e), specific flexural modulus (f)

Flexural modulus (Figure 7a) showed a linear increase of 28.2%, approximated by Eq. (4).

$$y = 11.979 \cdot ID + 2070.8, \; with \; R^2 = 0.9749 \tag{4}$$

At the same time, the flexural strength (Figure 7b), which can be calculated by Eq. (5) increased even more, resulting in a 38.1% difference between the lowest and highest ID.

$$y = 0.4843 \cdot ID + 51.314, with\ R^2 = 0.9854 \quad (5)$$

The gap between total energy absorption (EA_t) and energy absorption at failure (EA_f) is shown to be growing linearly from 0.049 MJ/m^3 for 20%-ID to 2.445 MJ/m^3 for 100% ID (Figure 7c) which corresponds to the evolution of the type of fracture (Figure 6a) from quasi-brittle to the ductile one, respectively. The EA_t follows Eq. (6), and EA_f can be calculated according to Eq. (7).

$$y = 0.0492 \cdot ID + 0.1632,\ with\ R^2 = 0.9777 \quad (6)$$

$$y = 0.0201 \cdot ID + 0.8575,\ with\ R^2 = 0.9935 \quad (7)$$

Strain at strength is the only one of the properties that does not have a linear behavior (see Figure 7d), but a polynomial one, and can be approximated by Eq. (8). It has a small increase from 3.3% to 4.4% from the lowest to the highest ID, respectively.

$$y = -0.0002 \cdot ID^2 + 0.0357 \cdot ID + 2.6655,\ with\ R^2 = 0.9886 \quad (8)$$

For the calculation of specific flexural strength and the specific flexural modulus were used values from Figure 7a and b divided by the measured density. 20%-ID is shown to be the optimal infill density for specific flexural strength, and 60%-ID is the worst one (Figure 7e). The increase from worst to best ID in specific flexural strength is 10.8%. In Figure 7f, it can be seen that the specific flexural modulus is decreasing polynomial with the increase of ID. Therefore, the 20%-ID has the highest specific flexural modulus and the 100%-ID has the lowest one.

4. Conclusions

The flexural behavior of Fused Filament Fabrication (FFF)-printed Polylactic Acid (PLA) parts was investigated in the present paper. The following were found:

- The increase in infill density (ID) leads to a linear increase of all properties, except for the strain at strength, where it shows a polynomial increase.
- The biggest increase, in the 20–100% ID range, is noted for energy absorption (75.1%), and the smallest for strain at strength (24.5%).
- Compressive modulus and compressive strength show an increase of 28.2% and 38.1%, respectively.
- The measured mass of the samples is slightly lower (6.5%) than the theoretical one.
- The samples with low ID showed a quasi-brittle fracture, and with the increase of ID this changed to a ductile one.
- By using specific strength (strength-to-density ratio), it was found that the optimum ID is 20%, and the weakest is 60%.

Acknowledgement: This work was supported by a grant of the Ministry of Research, Innovation and Digitization, CNCS -UEFISCDI, project number PN-IV-P1-PCE-2023-1446, within PNCDI IV.

Funding Statement: The authors received no specific funding for this study.

Author Contributions: The authors confirm contribution to the paper as follows: study conception and design: Ion Miron, Emanoil Linul; data collection: Ion Miron, Cristina Vălean; analysis and interpretation of results: Ion Miron, Cristina Vălean, Emanoil Linul; draft manuscript preparation: Ion Miron, Cristina Vălean, Emanoil Linul. All authors reviewed the results and approved the final version of the manuscript.

Availability of Data and Materials: The data that support the findings of this study are available from the corresponding author, [E.L.], upon reasonable request.

Ethics Approval: Not applicable.

Conflicts of Interest: We confirm that there are no known conflicts of interest associated with this publication and there has been no significant financial support for this work that could have influenced its outcome.

References

1. Enache IC, Cristina IM, Chivu OR, Mates I, Ionita E, Geambasu G. The influence of 3D printing parameters on the mechanical behavior of PLA. Mater Plast. 2024;61(1):82–92. doi:10.37358/mp.24.1.5704.
2. Raja S, Praveenkumar V. Optimizing additive manufacturing parameters for graphene-reinforced PETG impeller production: a fuzzy AHP-TOPSIS approach. Results Eng. 2024;24(11):103018. doi:10.1016/j.rineng.2024.103018.
3. Zisopol DG, Minescu M, Iacob DV. A Study on the Influence of FDM Parameters on the Tensile Behavior of Samples made of PET-G. Eng Technol Appl Sci Res. 2024;14(2):13487–92. doi:10.48084/etasr.6949.
4. Liu Z, Wang Y, Wu B, Cui C, Guo Y, Yan C. A critical review of fused deposition modeling 3D printing technology in manufacturing polylactic acid parts. Int J Adv Manuf Technol. 2019;102(9):2877–89. doi:10.1007/s00170-019-03332-x.
5. Vălean C, Orbulov IN, Kemény A, Linul E. Low-cycle compression-compression fatigue behavior of MEX-printed PLA parts. Eng Fail Anal. 2024;161(18):108335. doi:10.1016/j.engfailanal.2024.108335.
6. Zisopol DG, Minescu M, Iacob DV. A study on the influence of FDM parameters on the compressive behavior of PET-G Parts. Eng Technol Appl Sci Res. 2024;14(2):13592–7. doi:10.48084/etasr.7063.
7. Braileanu PI, Calin A, Dobrescu TG, Pascu N-E. Comparative examination of friction between additive manufactured plastics and steel surface. Materiale Plastice. 2023;60(3):48–57. doi:10.37358/mp.23.3.5675.
8. Vălean C, Linul E, Palomba G, Epasto G. Single and repeated impact behavior of material extrusion-based additive manufactured PLA parts. J Mater Res Technol. 2024;30(13):1470–81. doi:10.1016/j.jmrt.2024.03.150.
9. Manole CST, Braileanu PI, Dobrescu TG, Chiscop F. Custom humeral joint prostheses using additive manufacturing and biocompatible smart materials. Mater Plast. 2023;60(3):19–30. doi:10.37358/mp.23.3.5672.
10. Zisopol DG, Portoacă A, Tănase M. Improving the impact resistance through annealing in PLA 3D printed parts. Eng Technol Appl Sci Res. 2023;13(5):11768–72. doi:10.48084/etasr.6281.
11. Vălean C, Baban M, Rajak DK, Linul E. Effect of multiple process parameters on optimizing tensile properties for material extrusion-based additive manufacturing. Constr Build Mater. 2024;414(18):135015. doi:10.1016/j.conbuildmat.2024.135015.
12. Garbatov Y, Scattareggia Marchese S, Epasto G, Crupi V. Flexural response of additive-manufactured honeycomb sandwiches for marine structural applications. Ocean Eng. 2024;302:117732. doi:10.1016/j.oceaneng.2024.117732.
13. Krzikalla D, Měsíček J, Halama R, Hajnyš J, Pagáč M, Čegan T, et al. On flexural properties of additive manufactured composites: experimental, and numerical study. Compos Sci Technol. 2022;218(2):109182. doi:10.1016/j.compscitech.2021.109182.

14. Maqsood N, Rimašauskas M. Delamination observation occurred during the flexural bending in additively manufactured PLA-short carbon fiber filament reinforced with continuous carbon fiber composite. Results Eng. 2021;11:100246. doi:10.1016/j.rineng.2021.100246.
15. Rebenaque AG, González-Requena I. Study of bending test of specimens obtained through FDM processes of additive manufacturing. Procedia Manuf. 2019;41:859–66. doi:10.1016/j.promfg.2019.10.008.
16. Yousefi Kanani A, Kennedy A. Experimental and numerical analysis of additively manufactured foamed sandwich beams. Compos Struct. 2023;312(7):116866. doi:10.1016/j.compstruct.2023.116866.
17. Atakok G, Kam M, Koc HB. Tensile, three-point bending and impact strength of 3D printed parts using PLA and recycled PLA filaments: a statistical investigation. J Mater Res Technol. 2022;18:1542–54. doi:10.1016/j.jmrt.2022.03.013.
18. Djokikj J, Tuteski O, Doncheva E, Hadjieva B. Experimental investigation on mechanical properties of FFF parts using different materials. Procedia Struct Integr. 2022;41(1):670–9. doi:10.1016/j.prostr.2022.05.076.
19. Vãlean C, Marsavina L, Linul E. Compressive behavior of additively manufactured lightweight structures: infill density optimization based on energy absorption diagrams. J Mater Res Technol. 2024;33(18):4952–67. doi:10.1016/j.jmrt.2024.10.143.
20. Vãlean C, Linul E, Rajak DK. Compressive performance of 3D-printed lightweight structures: infill pattern optimization via multiple-criteria decision analysis method. Results Eng. 2025;25(1):103936. doi:10.1016/j.rineng.2025.103936.
21. Lendvai L, Fekete I, Jakab SK, Szarka G, Verebélyi K, Iván B. Influence of environmental humidity during filament storage on the structural and mechanical properties of material extrusion 3D-printed poly(lactic acid) parts. Results Eng. 2024;24:103013. doi:10.1016/j.rineng.2024.103013.
22. Hiremath S, Dsouza JF, Chiniwar DS, Vishwanatha HM, Mallikarjuna B. Exploring the impact of epoxy coated 3D-Printed polymers on surface roughness and mechanical behavior: an experimental and numerical study. Results Eng. 2024;23(3):102779. doi:10.1016/j.rineng.2024.102779.
23. Rahatuzzaman M, Mahmud M, Rahman S, Hoque ME. Design, fabrication, and characterization of 3D-printed ABS and PLA scaffolds potentially for tissue engineering. Results Eng. 2024;21(10):101685. doi:10.1016/j.rineng.2023.101685.
24. Figueroa Romero G, Maldonado SR, Arciniaga LF, Gonzales DA, Villalobos EB, Potter BG, et al. Polymer-ceramic composites for fused deposition modeling of biomimetic bone scaffolds. Results Eng. 2024;23(10):102407. doi:10.1016/j.rineng.2024.102407.
25. ISO178:2019. Plastics—Determination of flexural properties. 6th ed. Geneva: International Organization for Standardization; April 2019. Available from: https:/standards.iteh.ai/catalog/standards/sist/6d9ee8ed-eaf6-49f6-b83bbd615d3367df/iso-178-2019.

Received: 10 October 2024; Accepted: 17 May 2025; Published: 30 September 2025